High performance MWIR type-II superlattice detectors

Henk Martijn, Carl Asplund, Rickard Marcks von Würtemberg, Hedda Malm
IRnova AB Electrum 236, SE-164 40 Kista, Sweden

ABSTRACT

A VGA format type-II superlattice focal plane array (FPA) for the mid-wave infrared (MWIR) atmospheric window has been designed, manufactured and characterized. The detector material is based on a heterojunction structure with a barrier that effectively decreases the Shockley-Read-Hall based component of the dark current. A very effective passivation method has been used which successfully inhibits all surface leakage currents. The barrier structure has a 50 % cutoff at 5 µm and 65 % quantum efficiency without antireflective coating. The dark current density is 3×10^{-6} A/cm^2 at -0.05 V bias and 120 K. The optical cavity of the detector has been optimized for maximum capture of available light in the MWIR window. A focal plane array with 640 by 512 pixels and 15 µm pitch was processed based on this barrier structure. High-quality imagery in a system with high F-number will be presented.

Keywords: type II superlattice, heterostructure, MWIR, photodetector, InAs/GaSb, M-structure

1. INTRODUCTION

In the 1980s, Smith and Maihiot [1] proposed type-II InAs/GaSb based strained layer superlattices (SLS) for infrared (IR) detection. SLS or also called T2SL (Type II SuperLattice), is a material / technology that can be used to make high quality cooled infrared photon detectors with a cut-off wavelength ranging from 2 µm to 30 µm. This covers the SWIR, MWIR, LWIR and VLWIR wavelength bands, loosely defined as 2-3 µm, 3-5 µm, 8-12 µm and >12 µm, respectively. Commercially available IR detectors in the MWIR region are mercury cadmium telluride (MCT) and bulk InSb photon detectors. However Type-II superlattices have interesting properties compared to current technologies. T2SL benefits from a larger carrier effective mass, compared to the state-of-the-art MCT technology, leading to reduced tunneling currents [1] [2] and significant reduction of Auger recombination rate [3]. This in its turn leads to higher operating temperatures. These advantages however, have not yet experimentally been shown in T2SL, mainly because other dark current mechanisms related to defects in the material still dominate. Therefore one of the challenges for T2SL to reach its full potential is to either eliminate the defects or work around them. Fortunately the InAs/GaSb/AlSb material system gives a very large design freedom that can be utilized to realize more complex device structures with extra features intended to reduce the undesirable dark current mechanisms.

In simple homojunction devices a lightly doped "intrinsic" region (*i*) is sandwiched between heavier doped *p*- and *n*-type contact layers. The *i* absorber region is preferably *p* doped as holes have lower mobility than electrons and it is therefore beneficial to have the latter as minority carriers. Under light reverse bias the space charge region arises almost completely in the lower doped *i* layer. Experimental measurements show that the dark current is up to high temperatures dominated by g-r current in this type of structures [4] [5]. The source of g-r current is Shockley-Read-Hall (SRH) centers in the depletion region; typically caused by defects, impurities or interface states. In the general case the net generation rate can be described by the following classical expression [6] [7]:

$$G - R = (n_i^2 - np)/((n + n_1)\tau_{p0} + (p + p_1)\tau_{n0}), \quad (1)$$

where G is the generation rate, R is the recombination rate, and n_1 and p_1 are the electron and hole densities in the material when the Fermi level is equal to the energy level of the SRH centers in the bandgap. τ_{p0} and τ_{n0} are the electron and hole lifetime respectively. For a homojunction device the SRH generation currents are directly proportional to the width of the space charge region, W. The relation to the doping levels is then as follows:

$$J_{SRH} = (G - R)qW \text{ , where } W \propto \sqrt{(N_A + N_D)/N_A N_D} \quad (2)$$

Infrared Technology and Applications XXXIX, edited by Bjørn F. Andresen, Gabor F. Fulop,
Charles M. Hanson, Paul R. Norton, Proc. of SPIE Vol. 8704, 87040Z · © 2013 SPIE
CCC code: 0277-786X/13/$18 · doi: 10.1117/12.2016602

Downloaded From: http://spiedigitallibrary.org/ on 06/17/2013 Terms of Use: http://spiedl.org/terms

In the case of much lower absorber doping $N_{A,}$ as compared to $N_{D,}$ this can be simplified further to:

$$J_{SRH} \propto 1/\sqrt{N_A} \tag{3}$$

In other words, in a homojunction device the SRH current varies slowly and predictably with absorber doping N_A.

As is clear from Eq. (1), for midgap defect levels in the depletion region the g-r current is proportional to the intrinsic carrier concentration n_i. The intrinsic carrier concentration is a strong function of the bandgap energy, so in this work we use a heterojunction design similar to [8] where the most of the deletion region resides in the higher bandgap material. Due to the fact that only a minor part of the depletion region extends into the absorber, the g-r current is much reduced, but the dependence on the absorber doping level is much stronger than in Eq. (3), as we shall see in Section 3.2.

In this work the improvements and optimizations that can be made on a heterojunction design for the MWIR wavelength band are studied. We will look in more detail at optical response, dark current improvements and passivation methods. The target is a focal plane array with 640 by 512 pixels on 15µm pitch operating at 120 K; to be used in systems with F/4 aperture.

2. EXPERIMENTAL

The baseline detector material used in this work, "Design A", is grown on n-type (Te-doped) GaSb (100) substrates using solid source molecular epitaxy (MBE). The material consists of a 0.3 µm lattice matched $InAs_{0.91}Sb_{0.09}$ etch-stop layer, followed by 0.7 µm heavily Si-doped *n*-type "M-superlattice" (M-SL) bottom contact, 0.5 µm lightly doped n-type M-SL, 3 µm weakly doped *p*-type SL absorber, 0.1 µm of an intermediate bandgap heavily Be-doped *p*-type SL, and finally a 0.1 µm thick heavily Be-doped *p*-type GaSb contact layer. The M-SL periods consist of InAs/GaSb/AlSb/GaSb in the proportions 10/1/4/1 ML, whereas the absorber SL consists of 9.5 ML InAs / 11.5 ML GaSb. The top and bottom contacts are doped to 2×10^{18} and 6×10^{17} cm^{-3}, respectively, whereas the doping concentration in the absorber is 1×10^{16} cm^{-3} (*p*-type); see Figure 1.

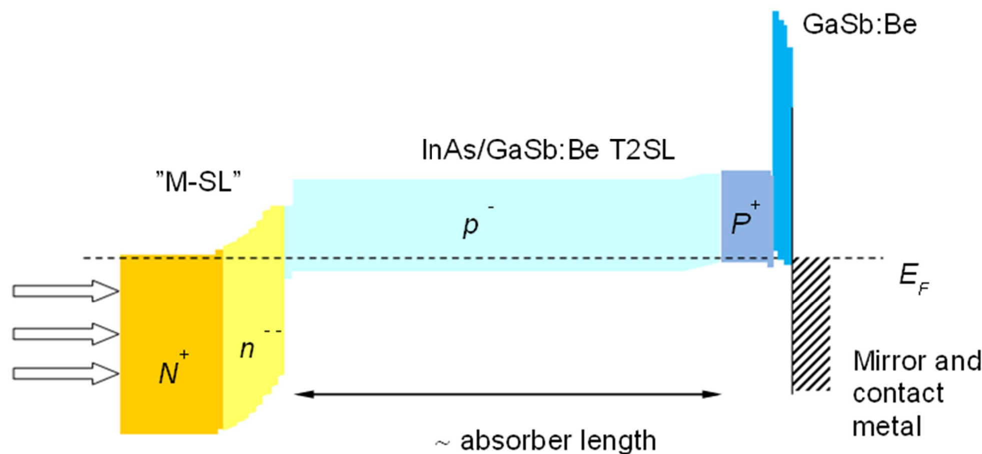

Figure 1 Overview of the detector structure under zero bias condition

Downloaded From: http://spiedigitallibrary.org/ on 06/17/2013 Terms of Use: http://spiedl.org/terms

Design B and Design C are variants of the baseline design. They vary in absorber thickness, cut-off wavelength and absorber doping level, see Table 1.

Table 1 Summary of the different designs used in this work with varying absorber thickness, cut-off wavelength and absorber doping level.

	Absorber thickness	Absorber Super Lattice	Absorber doping **(cm^{-2})**
Design A	3 µm	9.5 ML InAs / 11.5 ML GaSb	1.1×10^{16}
Design B	4 µm	10 ML InAs / 11.5 ML GaSb	1.1×10^{16}
Design C	4 µm	10 ML InAs / 11.5 ML GaSb	3.3×10^{16}

Standard III/V-processing was performed on Design A epi material to produce a detector array with 640×512 pixels and a pixel pitch of 15 µm; mesas were formed using a combination of dry and wet etching [9], after which they were passivated using polymer based passivation. Mirror and contact metal was evaporated and after dicing the detector material was hybridized to an ISC0403 readout. Finally, the substrate was fully removed. A fill factor of 81% was achieved using this process. The same process was also used to fabricate devices with a number of single pixels of different sizes, both with polymer and dielectric passivation. These devices were used to evaluate dark current behavior and optical response. All results reported in this paper were obtained for devices without antireflective (AR) coating.

The quantum efficiency (QE) spectrum was measured using a dispersive spectrometer with a calibrated photon flux entering through the substrate, or – in the case of removed substrate – through the bottom contact material. A lock-in amplifier was used to suppress noise and background signal.

The generation-recombination rates were modeled by solving the standard semiconductor drift-diffusion equations in 1D. Convergence of self-consistent solutions for low temperatures was achieved by increasing the numerical precision beyond the 64 bits representation of a standard double precision floating point number.

An 8×8 k.P transfer-matrix envelope function approximation simulator was used to model the superlattice band structure [10]. Material data, including band offsets were taken from ref. [11]

Downloaded From: http://spiedigitallibrary.org/ on 06/17/2013 Terms of Use: http://spiedl.org/terms

3. RESULTS

3.1 Optical optimization

Reference design A has a cut-off at 4.8 µm. This is slightly too short to take full advantage of all photons available in the MWIR band; especially considering that the photon flux or Planck radiation of a room temperature body increases rapidly for longer wavelengths. To increase the cut-off wavelength, the InAs superlattice layer in the absorber was therefore increased by 0.5 ML to 10 ML. To also improve the quantum efficiency the absorber thickness was increased to 4 µm.

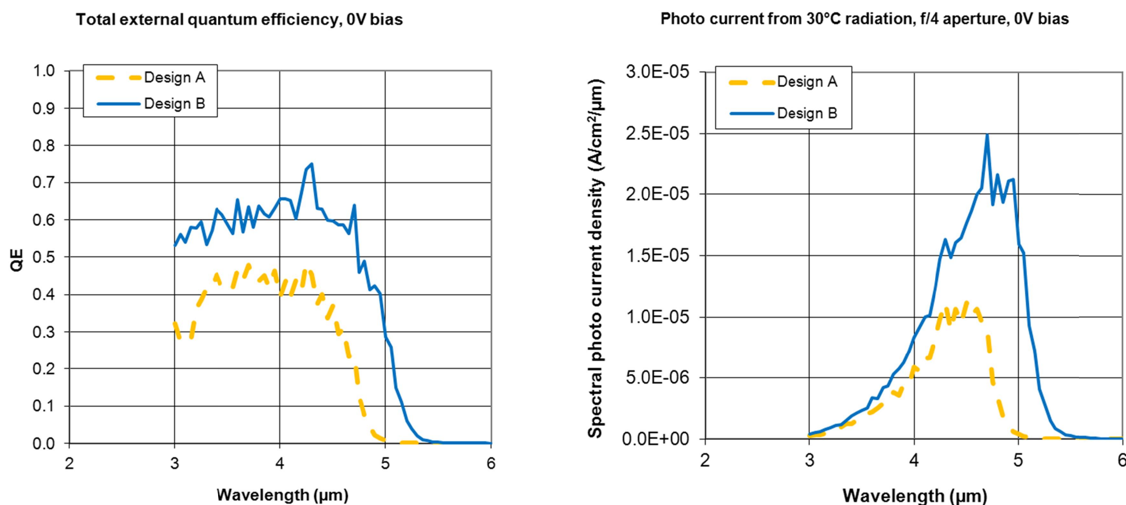

Figure 2 External quantum efficiency and spectral photocurrent density of Design A and Design B. No antireflective coating was applied.

The increase of the absorber thickness resulted in an increase of QE from 40 % to 60 %; see Figure 2. The increase of the cut-off wavelength to 5.1 µm corresponds very well with the expected shift as predicted by k.P simulations, validating the usefulness of the used k.P model. If we look at the total photocurrent integrated over the 3 to 5 µm interval for a typical application (30°C background F/4) we see a two-fold increase due to these improvements in the detector design.

3.2 Dark Current

In a correctly designed heterojunction device, with a lower doping level in the barrier than in the absorber, most of the space charge region lies in the higher bandgap material. In the high bandgap barrier, the generation rate is much lower than in the absorber region, hence only the tail of the depletion region extending into the absorber region will contribute to the SRH current. Because the assumptions leading to eq. (3) do not hold, we have to rely on simulations to predict the generation rate. The extension of the depletion region into the absorber will decrease rapidly with increasing absorber doping N_A. The simulation results in Figure 3 to Figure 5 show this very clearly: a 3 fold increase of the absorber doping leads to a very rapid decrease of the total net generation rate, by far more than the factor of $\sqrt{3}$ that would be expected from corresponding homojunction devices. The simulations show also clearly that the generation rate in the barrier (to the left of the 1.2 µm mark) can be neglected.

Downloaded From: http://spiedigitallibrary.org/ on 06/17/2013 Terms of Use: http://spiedl.org/terms

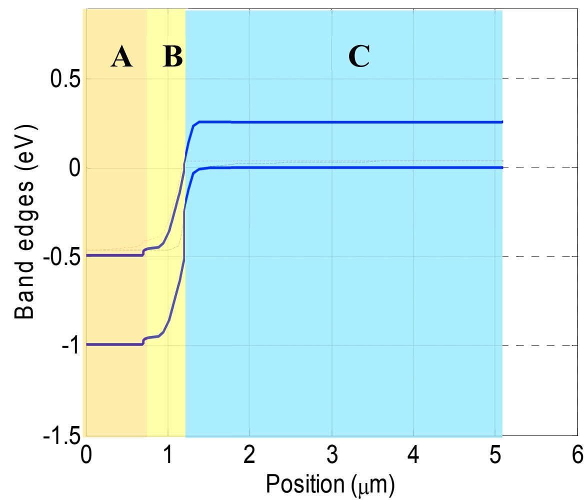

*Figure 3 Band alignment of Design B under reverse bias, Region **A** is the N^+ contact layer, **B** The n^{--} barrier and **C** the p^- absorber.*

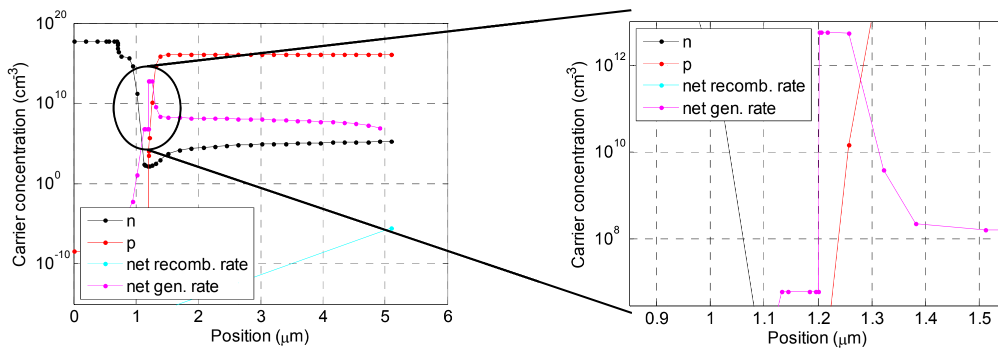

Figure 4 Design B, simulation of free carrier concentration in units of cm^{-3}, and net generation rate of electron-hole pairs in arbitrary units. The figure on the right is an enlargement of the interface between the barrier and the absorber.

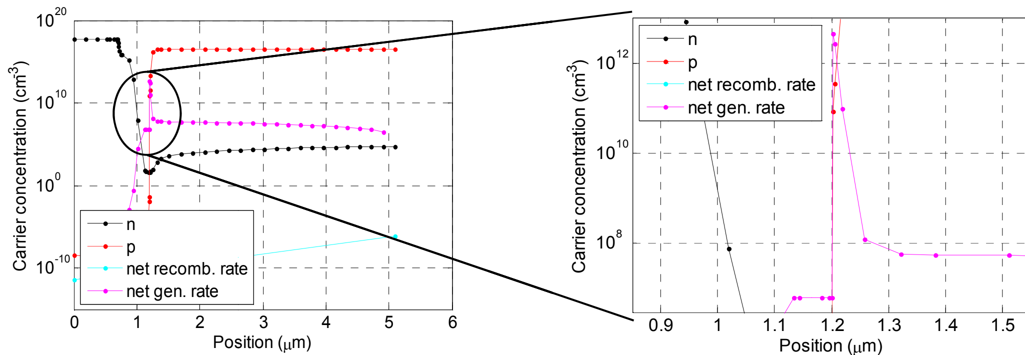

Figure 5 The same kind of simulation as in Figure 4, but for Design C. Please note that the y-axis scale is logarithmic, so the volume with any significant SRH current generation has decreased dramatically from that of Design B.

Downloaded From: http://spiedigitallibrary.org/ on 06/17/2013 Terms of Use: http://spiedl.org/terms

The simulations have been experimentally verified: two samples with single pixels of different sizes have been prepared. Design B based on material with nominal *p*-type absorber doping and Design C with 3 times higher doping.

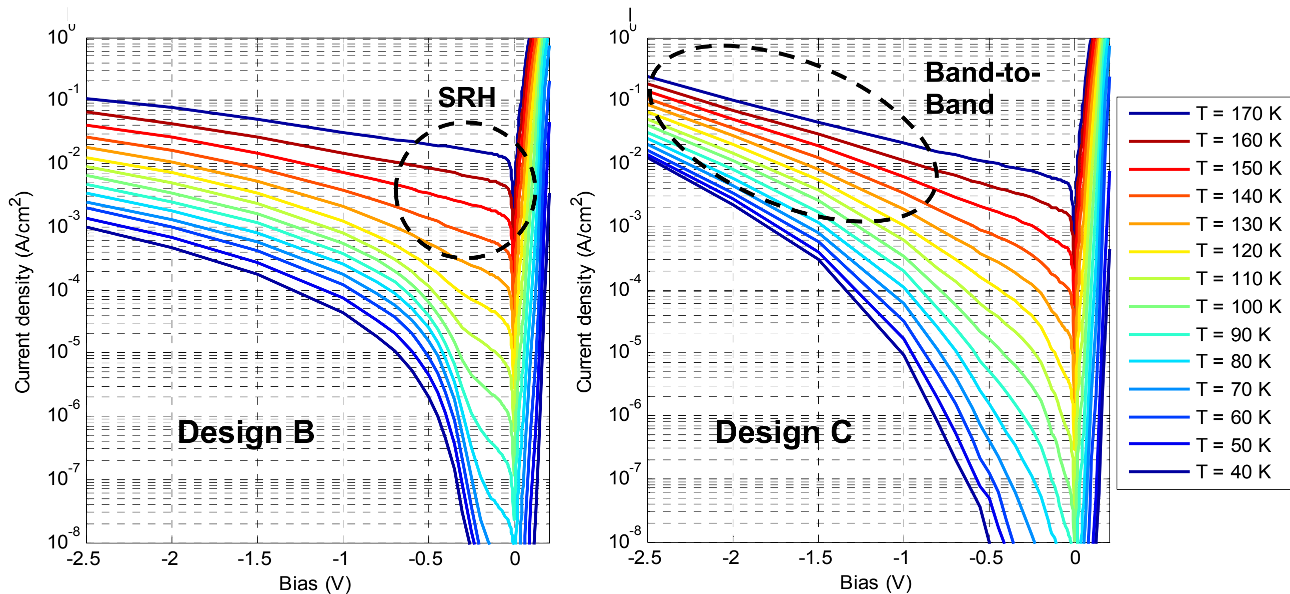

Figure 6 I-V characteristics for Design B (left) and Design C (right).

At low bias and high temperature the SRH currents are dominating in Design B, see Figure 6. At high bias however, the band-to-band tunneling is larger in Design C than in Design B. This can be explained by the higher field strength in the depletion area due to the higher p-doping. The higher band to band tunneling is of no importance because these devices are normally operated in a low bias regime where this component of the dark current is negligible.

The maximum RA product for these structures occur around -40 mV reverse bias and can be up to an order of magnitude larger than R_0A.

Table 2 RA and Dark current at 120 K operating temperature and -40 mV reverse bias

	RA (Ωcm^2)	Dark current Density (A/cm^2)
Design B	3×10^{3}	3×10^{-5}
Design C	20×10^{3}	3×10^{-6}

By increasing the doping, the RA product has increased with almost a factor 7 while the dark current has improved with a factor 10. The numbers for Design C suggest that it will be possible to operate this material with good performance at 120 K.

Downloaded From: http://spiedigitallibrary.org/ on 06/17/2013 Terms of Use: http://spiedl.org/terms

3.3 Passivation

To test the effect of different types of mesa etch and passivation processes, single pixel devices with different sizes and geometries were fabricated, starting with the epi material of Design A. As a reference we use a passivation process based on a polymer. The best results were obtained with a dielectric passivation.

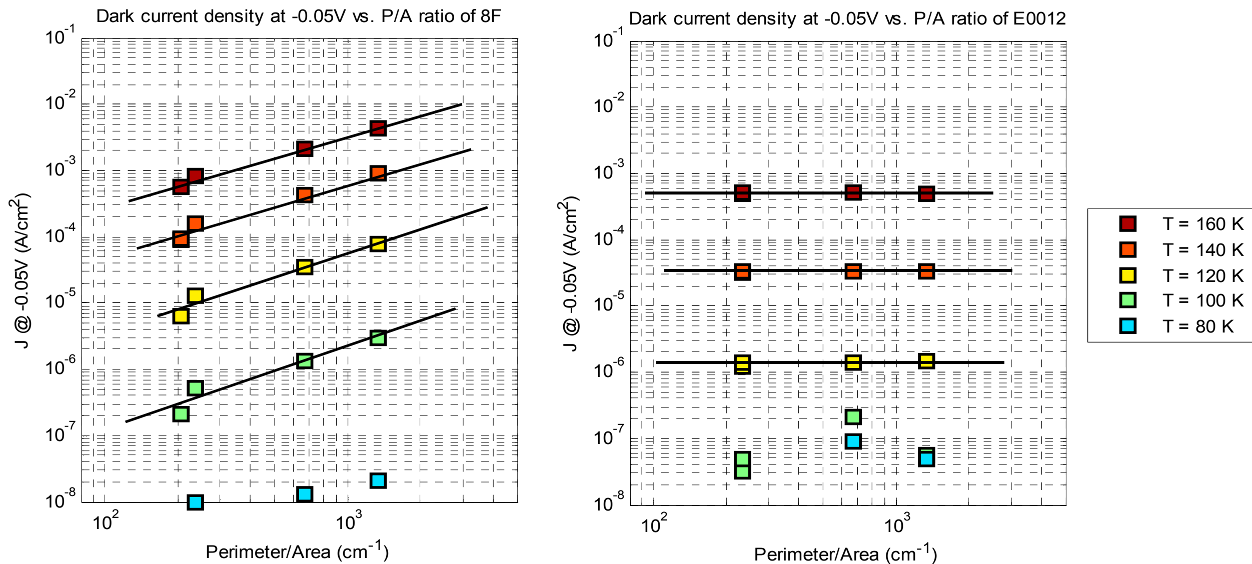

Figure 7 Dark current density as function of perimeter over area ratio for mesas with different sizes (170 µm, 60 µm and 30 µm) and temperatures. Left graph shows results for the polymer passivated mesas, right graph shows the results for the dielectric passivated mesas.

Figure 7 shows dark current density as function of perimeter over area. For a device exhibiting no surface leakage this relation should be a constant. As can be seen the polymer passivated samples showed a significant amount of edge currents while the dielectric passivated devices are completely bulk current dominated. When these results are extrapolated to even smaller 15 µm pixels, the improved passivation will give two orders of magnitude decrease of dark current. That corresponds to an improvement in operating temperature of 30 K.

The bulk dark current density of 1×10^{-6} A/cm^2 at 120 K is significantly lower than for homojunction devices of similar cutoff wavelength. However, there is still room for improvement. As shown by Chen et al. [12], with carefully optimized doping and band offsets the bulk dark current can reach the low 10^{-8} A/cm^2 range in similar heterojunction devices.

Downloaded From: http://spiedigitallibrary.org/ on 06/17/2013 Terms of Use: http://spiedl.org/terms

3.4 FPA results

Material from Design A was processed with polymer as passivation and hybridised to an ISC0403 readout circuit. The substrate was completely removed. A relatively high and not impressive NETD of 41 mK (50% well fill) was measured at 90 K with F/4 and 21 ms integration time. This is most likely due to the incomplete passiviation of this device and hence high surface leakage current and related noise on the mesa edges.

Figure 8 Images taken at 90 K with a 640 by 512 pixel, 15 µm pitch focal plane array processed from Design A material.

The images in Figure 8 taken at 90 K were two-point corrected and dead pixels have been removed. The operability is 99 % if pixels are marked as non-operating when the response deviates more than 7.5 % from its nearest neighbors or its NETD > 100 mK.

4. CONCLUSIONS

In conclusion, heterojunction detectors have been optimized with respect to dark current, optical response and surface passivation. High quality imaging of a 640 by 512 pixels FPA detector has been demonstrated. The performance is limited because not all improvements on dark current and optical response as described have been implemented in the demonstrator FPA. An optimized FPA should reach a NETD < 20 mK at an integration time < 10 ms. This FPA will be used in an IDCA (Integrated Dewar Cooler Assembly) with low weight, size and power.

ACKNOWLEDGEMENTS

The authors would like to acknowledge the support from the Swedish National Space Board and VINNOVA; Sweden's Innovation Agency who has made this work possible through the Center of excellence IMAGIC. The authors wish also to thank their colleagues at IRnova for processing of the samples.

REFERENCES

[1] Smith, D. L. and Mailhiot, C., "Proposal for strained layer type II superlattice infrared detectors," *J. Appl. Pyhs.,* vol. 62, pp. 2545-8, (1987).

[2] Mailhiot, C. and Smith, D. L., "Long-wavelength infrared detectors based on InAs-Ga1-xInxSb type-II superlattices," *Vac. Sci. Technol.7 A(2),* pp. 445-449, (1989).

[3] Mohseni, H., Litvinov, V. I. and Razeghi, M., "Interface-induced suppression of the Auger recombination in type-II InAs/GaSb superlattices," *Physical Review B,* vol. 58 (23), pp. 15378-80, (1998).

[4] Malm, H., Marcks von Würtemberg, R., Asplund, C., Martijn, H., Karim, A., Gustafsson, O., Plis, E. and Krishna, S., "Recent developments in type-II superlattice detectors at IRnova AB," *Proc. SPIE,* vol. 8353, p. 83530T, (2012).

Downloaded From: http://spiedigitallibrary.org/ on 06/17/2013 Terms of Use: http://spiedl.org/terms

[5] Asplund, C., Marcks von Würtemberg, R., Lantz, D., Malm, H., Martijn, H., Plis, E., Gautam, N. and Krishna, S., "Performance of mid-wave T2SL detectors with heterojunction barriers," *Infrared Physics and Technology,* in press, http://dx.doi.org/10.1016/j.infrared.2012.12.004, (2012).

[6] Shockley, W. and Read, W. T., "Statistics of the Recombinations of Holes and Electrons," *Phys. Rev.,* vol. 87, pp. 835-842, (1952).

[7] Hall, R. N., "Electron-Hole Recombination in Germanium," *Phys. Rev.,* vol. 87, p. 387, (1952).

[8] Abdollahi Pour, S., Huang, E. K., Chen, G., Haddadi, A., Nguyen, M. and Razeghi, M., "High operating temperature midwave infrared photodiodes and focal plane arrays based on type-II InAs/GaSb superlattices," *Appl. Phys. Lett. 98,* p. 143501, (2011).

[9] Chaghi, R., Cervera, C., Aït-Kaci, H., Grech, P., Rodriguez, J. B. and Christol, P., "Wet etching and chemical polishing of InAs / GaSb superlattice photodiodes," *Semicond. Sci. Technol. 24,* p. 065010, (2009).

[10] Szmulowicz, F., "Numerically stable secular equation for superlattices via transfer-matrix formalism and application to InAs/In0.23Ga0.77Sb and InAs/In0.3Ga0.7Sb/GaSb superlattices," *Phys. Rev. B,* vol. 57, p. 9081, (1998).

[11] Vurgaftman, I., Meyer, J. R. and Ram-Mohan, L. R., "Band parameters for III–V compound semiconductors and their alloys," J. Appl. Phys., vol. 89, p. 5815, (2001).

[12] Chen, G., B. Nguyen, M., Hoang, A. M., Huang, E. K., Darvish, S. R. and Razeghi, M., "Elimination of surface leakage in gate controlled type-II InAs/GaSb mid-infrared photodetectors," Appl. Phys. Lett., vol. 99, p. 183503, (2011).

Downloaded From: http://spiedigitallibrary.org/ on 06/17/2013 Terms of Use: http://spiedl.org/terms